Hybrid rGO@TiO2/CN Nanocomposite

Subjects: Engineering, Chemical

Contributor: Matejka Podlogar

The three-component hybrid (rGO/TiO2/CN) nanocomposite was prepared in order to enhance the photocatalytic properties of anatase TiO2 nanoparticles (NPs) under solar-like irradiation. The rGO/TiO2/CN was prepared in a mixture of the reduced graphene oxide (rGO, 8 wt%), anatase TiO2 nanoparticles (NPs), and graphitic carbon nitride (g-C3N4, 16 wt%).

graphitic carbon nitride | reduced graphene oxide | hydrothermal synthesis

1. Introduction

The presence of micropollutants on a large scale, particularly in virtually every aquatic ecosystem, has become a major problem. The widespread presence of man-made products, such as pharmaceuticals, dyes, pesticides, plastics, etc., are being detected daily, and investigation into their damaging impact on the biosphere and even human health do not show any positive aspects either. Pollution reaches the environment by different pathways, most abundantly through wastewater treatment [1][2], where currently employed wastewater treatment plants (WWTP) proved ineffective in the decomposition of harmful complexes. Given the global significance of clean water resources, new processing solutions of wastewater are required. In order to meet today's requirements and quickly introduce new technologies, solutions must be highly efficient, inexpensive and easily up-scalable.

In the field of remediation and the environmental protection of water systems, photocatalysis has attracted a lot of attention in recent years. A seemingly effective approach for this global problem employs advanced oxidation processes (AOPs) in the presence of a catalyst. The term AOP is reserved for a highly effective purification reaction in water, where the production of hydroxyl radicals ($HO^{\bullet}$) directly assists the decomposition of harmful organic micropollutants [3][4].

As a catalyst, titanium dioxide (TiO_2) was employed already very early; however, its photocatalytic application is limited due to the high recombination rate of photogenerated charge carriers and efficiency for photodegradation under abundant sunlight. The latter is due to TiO_2's wide bandgap energy of 3.2 eV, which makes merely 5% of the sunlight energy effective for the reaction [5]. Given the importance of water remediation and in order to employ this fascinating, cheap, and harmless compound in other applications, many strategies have been implemented [6]. Tuning the band gap or reducing the recombination rate of the semiconductor by ion doping has been a known technique for decades. Today, catalytic limitations are being overcome by producing complex nanostructures where TiO_2 is coupled with metal or non-metal elements [7][8]. In these composites, heterostructures are introduced, which effectively tailor the bandgap width or recombination rate of electron-hole pairs. Such TiO_2-based nanocomposites

have been successfully fabricated and showed enhanced photocatalytic activity shifted into the visible, e.g., sunlight range [9]. The combination of more components into the system to reduce the bandgap width, however, reduce overall catalytic activity in comparison to a single bandgap excitation, and to avoid this pitfall, so-called Z-scheme photocatalytic systems are being considered lately [10]. This photocatalytic reaction can facilely be realized by introducing a metal sink into a two-semiconductor heterojunction, by using noble metal nanoparticles, for example [11]. Very promising and mostly cheaper, however, are composites of graphene oxide/TiO_2/graphitic carbon nitride [5][12][13].

Graphene-based materials are attractive and well covered throughout the literature [14]. Their unique 2D structure of covalently bonded carbon atoms into a honeycomb-like lattice makes them mechanically strong and conductive, and because only a single atomic layer can be stabilized, they have a huge surface area, which gives a high aspect ratio between the junctions and bulk components. Not much thicker are graphene oxide (GO) and reduced graphene oxide (rGO) [15], two-dimensional structures with similar high mechanical strength, superb electron mobility, and great specific surface area. In the catalytic process, a graphene-based material, more commonly (rGO), serves as an electron sink, which in addition also decreases the recombination rates of the semiconductor [16][17]. The rGO/TiO_2 nanocomposites can easily be prepared by the sol-gel and hydrothermal method, with simultaneous TiO_2 growth and GO reduction to rGO [18][19].

Graphitic carbon nitride (*g*-C_3N_4), which is also added to the rGO/TiO_2 composite, is a two-dimensional metal-free polymeric semiconductor. The *g*-C_3N_4 with s-triazine ring structure has been of interest to researchers due to its chemical, thermal, photochemical, and physical stability, as well as for its low bandgap energy of 2.7 eV [20]. Furthermore, the synthesis of *g*-C_3N_4 by the thermal treatment of nitrogen-rich precursors such as urea, dicyandiamide, melamine, and cyanamide [21] is cheap and simple. On the other hand, the main disadvantages, such as the fast recombination of photoinduced electron-hole pairs, renders its usefulness as a single photocatalyst [22].

The preparation of a three-component hybrid (rGO/TiO_2/CN) photocatalyst has been used for different photocatalytic reactions [5][12][13][23]. However, in our opinion, many more experiments will have to be performed to explore the full potential of this exciting new material. Among them are two areas, namely, different synthesis routes and the investigation of photocatalytic performances and the degradation rate of other micropollutants.

2. Characterization

Raman and FTIR analyses were used to identify the chemical bonding in the synthetized photocatalysts. **Figure 1**A shows the FTIR spectra of the prepared GO, rGO, and *g*-C_3N_4 samples. The GO sample shows three characteristic absorption peaks in 1721, 1041, and 1381 cm^{-1} attributed to several oxygen functional groups, i.e., C=O and C-O stretching, and C-OH bending. The stretching vibration at 1225 cm^{-1} is assigned to the C-O-C of the epoxy groups. The broad stretching vibration band of the hydroxyl group, O-H, associated with absorbed water molecules and alcohol groups, is represented as a broad peak at 3380 cm^{-1}. Typical absorption peaks of GO disappear in the rGO spectrum. There, the absorption peak at 1617 cm^{-1} is assigned to the skeleton vibration of

less-oxidized graphitic materials, C=C. Comparison between the rGO spectrum and the GO spectrum shows that the reduction of GO by thermal treatment was significant. In the FTIR spectrum of the *g*-C_3N_4 sample, several strong peaks were observed in the 1200–1650 cm^{-1} region. Typical stretching vibrations of C-N heterocycles are represented at 1217, 1315, 1395, and 1452 cm^{-1}. The two bands appeared at 1541 and 1633 cm^{-1}, related to the stretching vibrations of C=N heterocycles, while the peaks located at 885 and 804 cm^{-1} arose from the characteristic breathing mode of tri-s-triazine rings units. All are characteristic for *g*-C_3N_4 material. The extra vibrational region between 3000–3300 cm^{-1}, although not directly related to the *g*-C_3N_4 structure, is commonly found in this compound [5][24], and can be associated with H_2O absorption and possible N-H bonds at the surface. **Figure 1**B shows characteristic functional vibrations of FTIR spectra of the prepared pure TiO_2 nanoparticles, TiO_2/rGO, TiO_2/CN nanocomposites, and the rGO@TiO_2/CN hybrid photocatalyst.

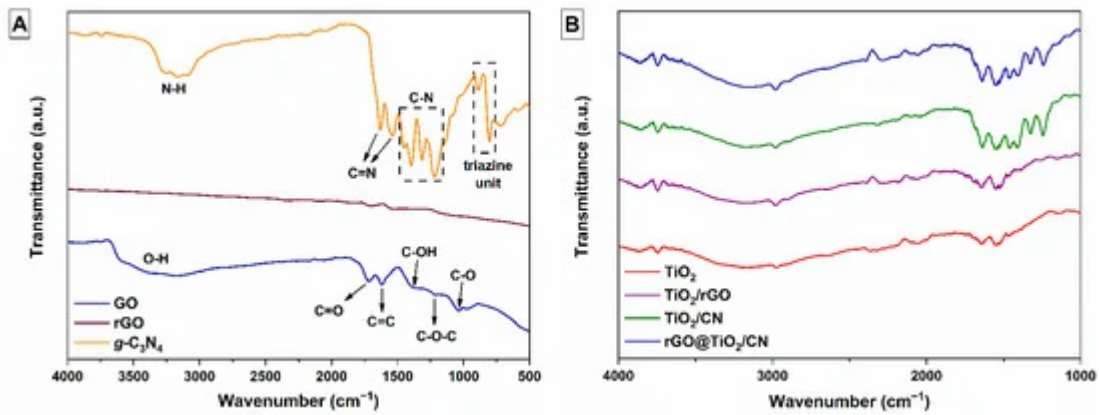

Figure 1. (**A**) FTIR spectra of as-prepared GO, rGO, and *g*-C_3N_4 materials and (**B**) pure TiO_2 nanoparticles, TiO_2/rGO, TiO_2/CN nanocomposites, and rGO@TiO_2/CN hybrid photocatalyst.

Raman spectra of pure TiO_2 nanoparticles, GO, thermally treated rGO, and the prepared rGO@TiO_2/CN hybrid material are displayed in **Figure 2**A. The typical bands of anatase TiO_2 are located at 147, 398, 517, and 641 cm^{-1}, which are attributed to the $Eg_{(1)}$, B_{1g}, A_{1g} + B_{1g}, and $E_{g(2)}$, respectively. The Raman spectrum of synthesized GO showed two typical peaks at the wavenumber of 1356 cm^{-1} and 1607 cm^{-1}, which corresponds to the D and G bands. The D band is associated with the in-plane sp^3 defects, while the G band represents in-plane vibrations of ordered sp^2-bonded carbon atoms in a two-dimensional hexagonal lattice. The D and G bands, after the hydrothermal reduction process, are shifted to the lower wavenumber at 1336 cm^{-1} and 1591 cm^{-1}. In the case of rGO, the D band got slightly larger with the reduction process, which increased the level of defects in the material, while the shifted G band indicates the re-graphitization process [25]. The Raman spectrum of the rGO@TiO_2/CN hybrid sample contained four characteristic bands of anatase phase of TiO_2 and two typical bands of rGO (D and G) The D and G bands in the prepared rGO@TiO_2/CN sample were found in the unchanged position as in the rGO sample, which suggests a reduction level similar to the pure GO reduction. As shown Raman spectrum of *g*-C_3N_4, a broad peak was observed between 1200–1800 cm^{-1}, which is similar to other reports [13][26]. Although two characteristic peaks, corresponding to D and G bands, should be resolved in this region, the obtained spectrum did not clearly express this feature. This was either because the excitation energy (633 nm excitation) was not optimal for the material [27], which could include defects, or because it was less crystalline. The intensity ratios of the D and

G bands (I_D/I_G), specifically, show the concentration of the sp^3 hybridized defects with respect to the sp^2-hybridized graphene domains. The hydrothermally prepared hybrid sample shows a higher intensity ratio (I_D/I_G = 1.10) in comparison with the synthesized GO sample (I_D/I_G = 1.02). According to [5], this suggests an interplay between TiO_2 intercalation and variation in defect concentration. Thus, Raman results better prove chemical interaction between graphene material and TiO_2 nanoparticles.

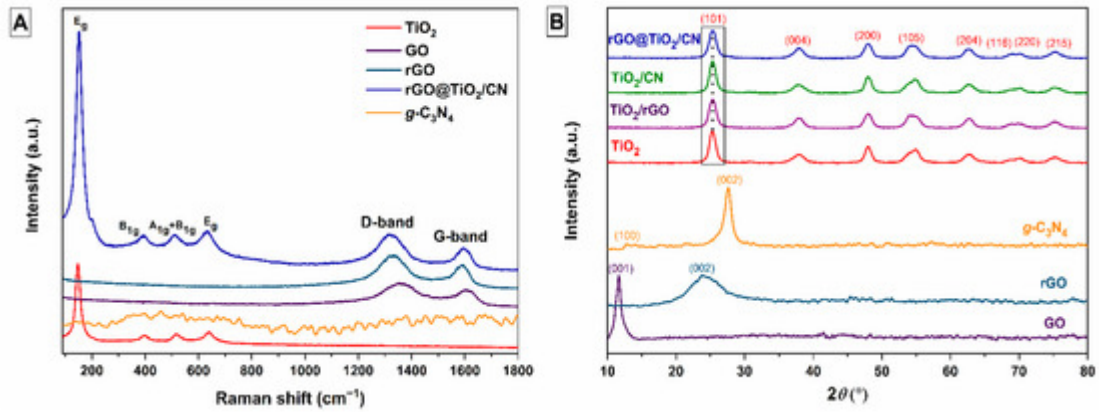

Figure 2. (**A**) Raman spectra of TiO_2, GO, rGO, *g*-C_3N_4, and rGO@TiO_2/CN nanocomposite, and (**B**) XRD patterns of the prepared materials.

Figure 2B shows the X-ray powder diffraction pattern of the prepared GO, rGO, *g*-C_3N_4, pure TiO_2 nanoparticles, TiO_2/rGO and TiO_2/CN nanocomposites, and rGO@TiO_2/CN hybrid samples. The GO pattern shows the strong diffraction peak at 2θ = 11.5° (001), which corresponds to an interlayer spacing of 0.76 nm and indicates the presence of oxygen functional groups in the GO sample [28]. In the rGO pattern, the broad diffraction peak is located at 2θ = 23.8° (002), which corresponds to an interlayer spacing of 0.74 nm. The decreased interlayer confirms the successful reduction of GO to rGO by applied hydrothermal treatment [19]. The *g*-C_3N_4 pattern contains two characteristic diffraction peaks according to JCPDS card no. 87-1526. The weaker peak located at 2θ = 12.8° (100) corresponds to an in-plane structural repeating of tri-s-triazine units and represents an interlayer spacing value of 0.69 nm. The sharp diffraction peak presented at 2θ = 27.5° (002) corresponds to the interlayer stacking of the conjugated aromatic segments with an interlayer spacing of 0.32 nm [20]. The nanoparticles synthesized by the simple hydrothermal method showed a crystalline nature, with 2θ peaks lying at 25.29° (101), 37.96° (004), 48.03° (200), 54.89° (105), 62.74° (204), 68.78° (116), 70.23° (220), and 75.35° (215). According to JCPDS card no. 21-1272, all the diffraction peaks of TiO_2 sample can be indexed to a pure anatase phase. These peaks are also observed in the prepared TiO_2/rGO, TiO_2/CN, and rGO@TiO_2/CN samples. Furthermore, in all the composite mixtures, XRD analysis failed to detect clear *g*-C_3N_4 or rGO presence, mostly due to a low mass percentage of the later, but also because carbon-based compounds lack long range order, which would be similar to TiO_2. Using the Scherrer equation, the crystalline domain size of the TiO_2 particle for all prepared samples was also estimated. The obtained crystallite size using (101) peak and a shape factor of 0.9 showed similar values around 7 nm (**Table 1**) for all samples.

Table 1. Calculated crystallite size (*D*, nm) of TiO_2 samples using the Scherrer equation.

Sample ID	*D*, nm
TiO_2	7.6
TiO_2/rGO	6.8
TiO_2/CN	7.5
rGO@TiO_2/CN	6.7

As revealed by the SEM (**Figure 3**A), pure TiO_2 crystals precipitated in the form of spheres. It was found that the particle size was smaller than 10 nm, which is consistent with the calculated crystallite size of 7.6 nm (**Table 1**). The SEM analysis of pure rGO and *g*-C_3N_4 materials pointed out to their known high specific surface area (**Figure 3**B,C), while imaging of the composite TiO_2/rGO, TiO_2/CN, and rGO@TiO_2/CN composite samples revealed similar TiO_2 crystals precipitated at the surface of the hybrid system (**Figure 3**D–F). Obviously, bigger aggregates in the composite samples arise most probably during the drying sequence and as is shown later, do not diminish degradation process. **Figure 4** shows the TEM image of the rGO@TiO_2/CN hybrid material, where the TiO_2 component is undoubtedly resolved, while carbon containing compounds are not so clear. However, the sheet of rGO and fiber-like *g*-C_3N_4 are obviously present, and EDS shows Ti, O, C, and N over the region of this hybrid material. The average size of anatase TiO_2 nanoparticles is around 6 nm.

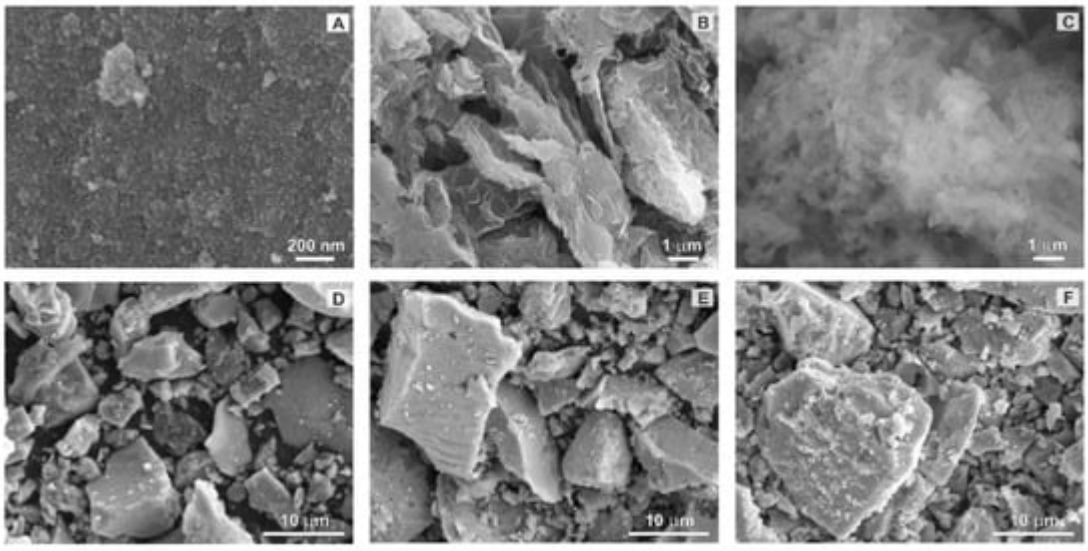

Figure 3. SEM images of (**A**) pure TiO_2 nanoparticles, (**B**) rGO, (**C**) *g*-C_3N_4, (**D**) TiO_2/rGO, (**E**) TiO_2/CN, and (**F**) rGO@TiO_2/CN.

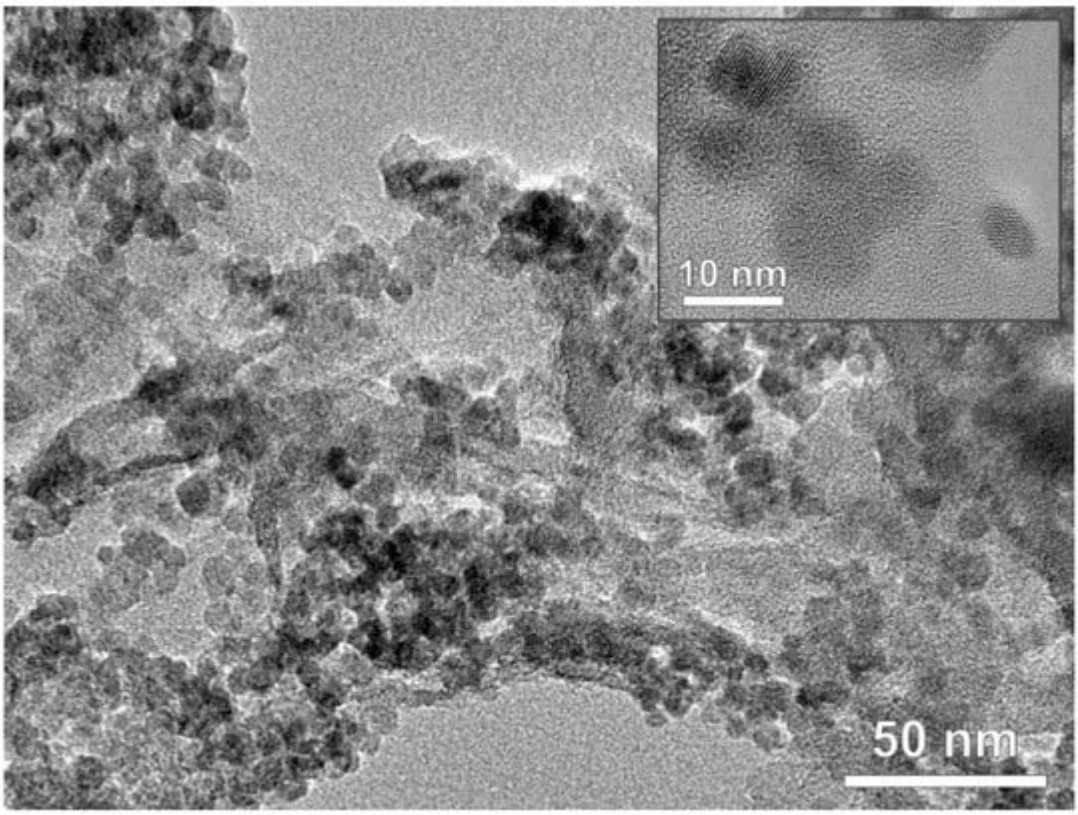

Figure 4. TEM image of rGO@TiO_2/CN nanocomposite and inset of anatase TiO_2 nanoparticles.

The specific surface area of the rGO@TiO_2/CN hybrid material was determined by the Brauner-Emmett-Teller (BET) method, and it was 185.82 m^2/g. The obtained result is higher than to the literature findings, based on similar preparation procedures for the rGO@TiO_2/CN hybrid [29].

The surface chemical composition and oxidation state of the as-prepared rGO@TiO_2/CN hybrid material were determined by XPS analysis, as shown in **Figure 5**. **Figure 5**A shows the full spectrum of characterized photocatalyst; Ti, O, C, and N peaks can be observed. Moreover, the peak intensities of Ti and O elements are clearly stronger than that of C and N, which corresponds to the obtained XRD results. The high-resolution spectrum of Ti 2p is shown in **Figure 5**B. The Ti 2p spectrum contains two symmetric peaks centered at 465.0 eV and 459.3 eV, which correspond to the Ti $2p_{1/2}$ and Ti $2p_{3/2}$. The obtained binding energy values correspond with Ti^{4+} in the TiO_2 chemical environments. The peak was determined at 456.7 eV, which can be attributed to the Ti-N bond due to the solid adhesion of TiO_2 on the *g*-C_3N_4 surface [18][30]. Based on this, **Figure 5**C shows the O 1s spectrum. The main peak is located at 530.5 eV, assigned to oxygen bonded to titanium (Ti-O-C), and a smaller peak around 531.3 eV, ordinarily attributed to hydroxyl groups in the structure of TiO_2. **Figure 5**D represents the N 1s spectrum, which can be fitted into two peaks with binding energies centered at 399.3 eV and 400.5 eV, assigned to the sp^2-hybridized nitrogen atom in the C-N=C group of triazine rings and sp^3-hybridized tertiary nitrogen N-$(C)_3$ in the heptazine unit [5]. The peak located at 401.4 eV, attributed to the C-N-H bond, which signifies the covalent bonding between rGO and *g*-C_3N_4, was not determined [30]. As shown in **Figure 5**E, the C1s spectrum could be divided into four peaks. The binding energies of the observed peaks at 284.5 and 287.2 eV can be assigned to the sp^2-hybridized carbon atom in the C-C bond and oxygen-containing epoxy/hydroxyl groups bond in the rGO

material. The observed peaks located at 285.9 eV and 288.6 eV correspond to the sp^2-bonded carbon in N-containing (C-N-C) and $(N)_2$-C=N in the aromatic ring of the *g*-C_3N_4 material [5][30]. Overall, the analysis of XPS results for the as-prepared rGO@TiO_2/CN hybrid material reveals successful interactions of *g*-C_3N_4 and rGO with TiO_2 nanoparticles and the pure form of the prepared hybrid sample.

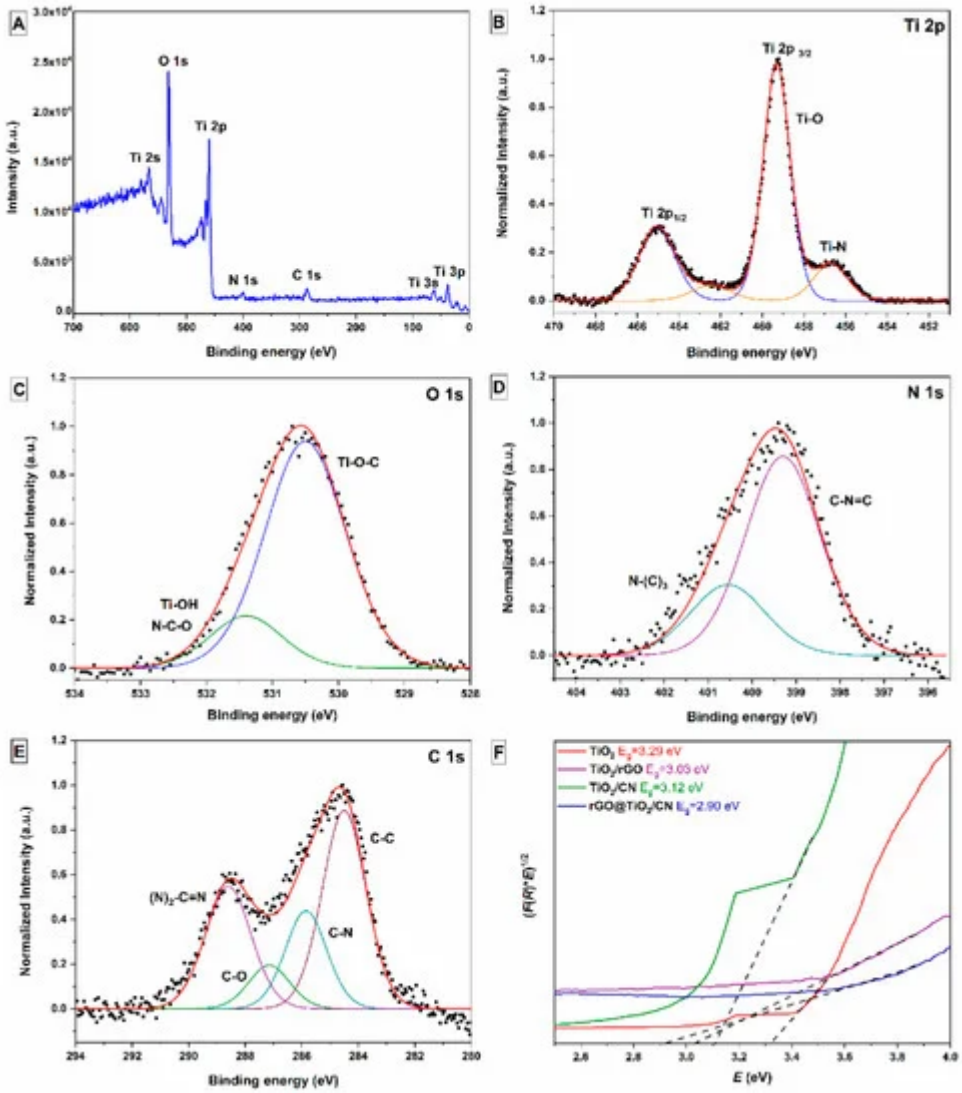

Figure 5. High-resolution XPS spectra of the as-prepared rGO@TiO_2/CN sample: (**A**) fully scanned spectrum, (**B**) Ti 2p, (**C**) O 1s, (**D**) N 1s, (**E**) C 1s, and (**F**) band gap energies (E_g) of prepared pure TiO_2 nanoparticles, TiO_2/rGO, and TiO_2/CN nanocomposites, and rGO@TiO_2/CN hybrid.

References

1. Mathon, B.; Ferreol, M.; Coquery, M.; Choubert, J.M.; Chovelon, J.M.; Miège, C. Direct photodegradation of 36 organic micropollutants under simulated solar radiation: Comparison with free-water surface constructed wetland and influence of chemical structure. J. Hazard. Mater. 2021, 407, 124801.

2. Oladoja, N.A.; Unuabonah, I.E. The pathways of microplastics contamination in raw and drinking water. J. Water Process Eng. 2021, 41, 102073.
3. Pedrosa, M.; Figueiredo, J.L.; Silva, A.M.T. Graphene-based catalytic membranes for water treatment—A review. J. Environ. Chem. Eng. 2021, 9, 104930.
4. Andreozzi, R.; Caprio, V.; Insola, A.; Marotta, R. Advanced oxidation processes (AOP) for water purification and recovery. Catal. Today 1999, 53, 51–59.
5. Lin, P.; Hu, H.; Lv, H.; Ding, Z.; Xu, L.; Qian, D.; Wang, P.; Pan, J.; Li, C.; Cui, C. Hybrid reduced graphene oxide/TiO2/graphitic carbon nitride composites with improved photocatalytic activity for organic pollutant degradation. Appl. Phys. A Mater. Sci. Process. 2018, 124, 510.
6. Rej, S.; Bisetto, M.; Naldoni, A.; Fornasiero, P. Well-defined Cu2O photocatalysts for solar fuels and chemicals. J. Mater. Chem. A 2021, 9, 5915–5951.
7. Assadi, M.H.N.; Hanaor, D.A.H. The effects of copper doping on photocatalytic activity at (101) planes of anatase TiO2: A theoretical study. Appl. Surf. Sci. 2016, 387, 682–689.
8. Doustkhah, E.; Assadi, M.H.N.; Komaguchi, K.; Tsunoji, N.; Esmat, M.; Fukata, N.; Tomita, O.; Abe, R.; Ohtani, B.; Ide, Y. In situ Blue titania via band shape engineering for exceptional solar H2 production in rutile TiO2. Appl. Catal. B Environ. 2021, 297, 120380.
9. Shehzad, N.; Tahir, M.; Johari, K.; Murugesan, T.; Hussain, M. A critical review on TiO2 based photocatalytic CO2 reduction system: Strategies to improve efficiency. J. CO2 Util. 2018, 26, 98–122.
10. Ma, L.; Jia, I.; Guo, X.; Xiang, L. High performance of Pd catalysts on bimodal mesopore for the silica catalytic oxidation of toluene. Chin. J. Catal. 2014, 35, 108–119.
11. Gao, H.; Zhang, P.; Hu, J.; Pan, J.; Fan, J.; Shao, G. One-dimensional Z-scheme TiO2/WO3/Pt heterostructures for enhanced hydrogen generation. Appl. Surf. Sci. 2017, 391, 211–217.
12. Das, S.; Mahalingam, H. Exploring the synergistic interactions of TiO2, rGO, and g-C3N4 catalyst admixtures in a polystyrene nanocomposite photocatalytic film for wastewater treatment: Unary, binary and ternary systems. J. Environ. Chem. Eng. 2019, 7, 103246.
13. Ibrahim, Y.O.; Hezam, A.; Qahtan, T.F.; Al-Aswad, A.H.; Gondal, M.A.; Drmosh, Q.A. Laser-assisted synthesis of Z-scheme TiO2/rGO/g-C3N4 nanocomposites for highly enhanced photocatalytic hydrogen evolution. Appl. Surf. Sci. 2020, 534, 147578.
14. Allen, J.M.; Vincent, T.C.; Richard, K.B. Honeycomb carbon: A Review of Graphene What is graphene ? Chem. Rev. 2010, 110, 132–145.
15. Erickson, K.; Erni, R.; Lee, Z.; Alem, N.; Gannett, W.; Zettl, A. Determination of the local chemical structure of graphene oxide and reduced graphene oxide. Adv. Mater. 2010, 22, 4467–4472.

16. Kovačić, M.; Perović, K.; Papac, J.; Tomić, A.; Matoh, L.; Žener, B.; Brodar, T.; Capan, I.; Surca, A.K.; Kušić, H.; et al. One-Pot Synthesis of Sulfur-Doped TiO2/Reduced Graphene Oxide Composite (S-TiO2/rGO) with Improved Photocatalytic Activity for the Removal of Diclofenac from Water. Materials 2020, 13, 1621.
17. Zouzelka, R.; Remzova, M.; Plsek, J.; Brabec, L.; Rathousky, J. Immobilized rGO/TiO2 photocatalyst for decontamination of water. Catalysts 2019, 9, 708.
18. Kocijan, M.; Ćurković, L.; Ljubas, D.; Mužina, K.; Bačić, I.; Radošević, T.; Podlogar, M.; Bdikin, I.; Otero-Irurueta, G.; Hortigüela, M.J.; et al. Graphene-Based TiO2 Nanocomposite for Photocatalytic Degradation of Dyes in Aqueous Solution under Solar-Like Radiation. Appl. Sci. 2021, 11, 3966.
19. Kusiak-Nejman, E.; Wanag, A.; Kapica-Kozar, J.; Kowalczyk, Ł.; Zgrzebnicki, M.; Tryba, B.; Przepiórski, J.; Morawski, A.W. Methylene blue decomposition on TiO2/reduced graphene oxide hybrid photocatalysts obtained by a two-step hydrothermal and calcination synthesis. Catal. Today 2019, 357, 630–637.
20. Bairamis, F.; Konstantinou, I.; Petrakis, D.; Vaimakis, T. Enhanced Performance of Electrospun Nanofibrous TiO2/g-C3N4 Photocatalyst in Photocatalytic Degradation of Methylene Blue. Catalysts 2019, 9, 880.
21. Rusek, J.; Paušová, Š.; Praus, P.; Krýsa, J. Immobilization of Exfoliated g-C3N4 for Photocatalytical Removal of Organic Pollutants from Water. Catalysts 2021, 11, 203.
22. Starukh, H.; Praus, P. Doping of graphitic carbon nitride with non-metal elements and its applications in photocatalysis. Catalysts 2020, 10, 1119.
23. Wang, J.; Sun, Y.; Fu, L.; Sun, Z.; Ou, M.; Zhao, S.; Chen, Y.; Yu, F.; Wu, Y. A defective g-C3N4/RGO/TiO2composite from hydrogen treatment for enhanced visible-light photocatalytic H2production. Nanoscale 2020, 12, 22030–22035.
24. Li, W.; Chen, Q.; Zhong, Q. One-pot fabrication of mesoporous g-C3N4/NiS co-catalyst counter electrodes for quantum-dot-sensitized solar cells. J. Mater. Sci. 2020, 55, 10712–10724.
25. Thirumalraj, B.; Rajkumar, C.; Chen, S.M.; Palanisamy, S. One-Pot Green Synthesis of Graphene Nanosheets Encapsulated Gold Nanoparticles for Sensitive and Selective Detection of Dopamine. Sci. Rep. 2017, 7, 41213.
26. An, T.; Tang, J.; Zhang, Y.; Quan, Y.; Gong, X.; Al-Enizi, A.M.; Elzatahry, A.A.; Zhang, L.; Zheng, G. Photoelectrochemical Conversion from Graphitic C3N4 Quantum Dot Decorated Semiconductor Nanowires. ACS Appl. Mater. Interfaces 2016, 8, 12772–12779.
27. Kang, Y.; Yang, Y.; Yin, L.C.; Kang, X.; Liu, G.; Cheng, H.M. An Amorphous Carbon Nitride Photocatalyst with Greatly Extended Visible-Light-Responsive Range for Photocatalytic Hydrogen Generation. Adv. Mater. 2015, 27, 4572–4577.

28. Choi, Y.-J.; Kim, E.; Han, J.; Kim, J.-H.; Gurunathan, S. A Novel Biomolecule-Mediated Reduction of Graphene Oxide: A Multifunctional Anti-Cancer Agent. Molecules 2016, 21, 375.
29. Hu, L.; Flanders, P.M.; Miller, P.L.; Strathmann, T.J. Oxidation of sulfamethoxazole and related antimicrobial agents by TiO2 photocatalysis. Water Res. 2007, 41, 2612–2626.
30. Hafeez, H.Y.; Lakhera, S.K.; Bellamkonda, S.; Rao, G.R.; Shankar, M.V.; Bahnemann, D.W.; Neppolian, B. Construction of ternary hybrid layered reduced graphene oxide supported g-C3N4-TiO2 nanocomposite and its photocatalytic hydrogen production activity. Int. J. Hydrog. Energy 2018, 43, 3892–3904.